CO Rebinding Kinetics to Myoglobin- and R-State-Hemoglobin-Doped Silica Gels in the Presence of Glycerol

Silvia Sottini,[†,‡] Cristiano Viappiani,*[,†,‡] Luca Ronda,[§] Stefano Bettati,[‡,#] and Andrea Mozzarelli[‡,§]

Dipartimento di Fisica, Università degli Studi di Parma, Parco Area delle Scienze 7/A, 43100 Parma, Italy; Dipartimento di Biochimica e Biologia Molecolare, Università degli Studi di Parma, Parco Area delle Scienze 23/A, 43100 Parma, Italy; Dipartimento di Sanità Pubblica, Università degli Studi di Parma, via Volturno 39, 43100 Parma, Italy; and Istituto Nazionale per la Fisica della Materia (INFM), c/o Dipartimento di Fisica, Università di Parma, parco area delle scienze 7A, 43100 Parma, Italy

Received: February 5, 2004; In Final Form: March 26, 2004

This study characterizes the CO rebinding kinetics after photodissociation of horse heart myoglobin (Mb) and human R-state hemoglobin (Hb) encapsulated in wet silica gels, in the presence of various concentrations of glycerol. The geminate yield for HbCO is scarcely affected by the gel matrix, indicating that the protein can fluctuate as in a homogeneous solution. On the contrary, the geminate yield for gel-embedded MbCO is much higher than that in solution, suggesting that the gel matrix inhibits the movements of the protein. The geminate yield for both proteins increases substantially with the addition of glycerol to the bathing solution. The observed kinetics could be rationalized using a simple three-state model. Rate constants have been modeled using a modified Kramers equation, which indicated that the gel exerts an internal friction on the elementary rate constants. The rate constant for geminate rebinding, k_{CA}, is essentially viscosity independent below ∼20 cP for both proteins. The internal friction for the ligand escape rate, k_{CS}, is much smaller and is found to be negligible for HbCO and ∼5 cP for MbCO. The activation barrier for k_{CS} increases with glycerol concentration in response to increased viscosity and reduced ligand solubility. The rate k_{SC} showed a complex behavior that reflects the opposing effects of viscosity and activity arising from molecular confinement and crowding. Accordingly, the corresponding activation barriers show a biphasic behavior, with a minimum at ≈40% glycerol for HbCO and at ≈75% glycerol for MbCO. The results highlight the potential of silica gel encapsulation for *in vitro* studies aimed to reproduce the crowded and confined environment experienced by proteins *in vivo*. The diverse response to encapsulation of Mb and Hb could actually reflect physiologically relevant functional properties escaping detection in the diluted solutions normally used for biophysical investigations.

Introduction

Myoglobin (Mb) and hemoglobin (Hb) continue to be used as model protein systems to understand how structure, dynamics, and reactivity correlate to give rise to the observed function. Among other methods, the rebinding of ligands to Mb and Hb in solution and in the crystalline state following laser photolysis has been extensively used over the years to understand the molecular mechanisms underlying protein−ligand interactions. After dissociation from the heme iron, ligands either rebind from the protein matrix in the so-called geminate recombination or escape into the solvent through exit channels that open transiently due to protein fluctuations. An impressive number of experimental works have characterized the rebinding kinetics under a variety of experimental conditions for both myoglobin[1−15] and hemoglobin.[12,16−25] The use of site-directed mutagenesis, combined with ultrafast kinetics, low-temperature X-ray crystallography, and molecular dynamics simulations, has provided a detailed picture of the kinetic pathways for ligand binding to Mb[26−30] and Hb.[31]

Rebinding of the photodissociated ligand to Mb occurs with a complex reaction resulting from protein relaxation and movements of the ligand within the protein.[28,29] After the work of Anfinrud and co-workers, it became clear that conformational relaxation in Mb is extended in time.[32,33] In viscous solutions at temperatures above the glass transition, where interconversion of substates and structural relaxation occur on the same time scale, the geminate rebinding kinetics to Mb can be described by a stretched exponential function.[34,35] Several pieces of experimental evidence have been accumulated[8−11,14,36] showing that this is the case even in aqueous solutions at physiological temperatures, where the structural relaxation was originally thought to be essentially complete before geminate binding begins.[21] Kinetic experiments show that the path of a CO molecule coming from the solvent (S) and moving to the binding site at the heme iron (A) can be approximated by a sequential model.[1−3]

Scheme 1

$$A \leftarrow B \rightleftarrows C \rightleftarrows D \rightleftarrows S$$

The location of CO in states B, C, and D has been suggested by crystallographic studies.[26−29] In state B, the CO remains in the heme cavity, approximately parallel to the heme plane, ∼4

* Address correspondence to this author at the Dipartimento di Fisica, Università degli Studi di Parma, Parco Area delle Scienze 7/A, 43100 Parma, Italy (fax +390521905223; telephone +390521905208; e-mail cristiano.viappiani@fis.unipr.it).

† Dipartimento di Fisica, Università degli Studi di Parma.

‡ Istituto Nazionale per la Fisica della Materia (INFM).

§ Dipartimento di Biochimica e Biologia Molecolare, Università degli Studi di Parma.

Dipartimento di Sanità Pubblica, Università degli Studi di Parma.

10.1021/jp049472g CCC: $27.50
Published on Web 05/20/2004

Å away from the iron. In state C, the CO most likely occupies the xenon cavity Xe4, whereas in state D the CO is in the largest cavity, Xe1. Although sequential models do not account for structural relaxation observed in kinetic experiments, it is possible to introduce corrections to this kinetic scheme by describing the structural relaxations overlapped to the geminate rebinding phase with a stretched exponential function.[7,9,36−38] Several kinetic schemes have been proposed to account for structural relaxation and multiple geminate intermediates.[11,14,39]

Studies on CO rebinding to Hb in solution at room temperature indicate that geminate rebinding can be treated as a first-order rate process, characterized by multiple exponential relaxations.[16,17,20,23,25] Time-resolved resonance Raman spectroscopy showed that tertiary relaxation occurred after photolysis of the CO complex.[40] The kinetics of the structural relaxation was investigated by optical absorption methods, showing the extended nature of the process.[16,20,21] The nonexponential geminate rebinding observed at room temperature in Hb could arise either from multiple geminate states, as in the original Frauenfelder model for myoglobin,[1,2] or from a slowing of geminate rebinding due to tertiary conformational relaxation.[21] To take into account the structural relaxation kinetics within a two-state allosteric model, Eaton and co-workers recently proposed an extension of a two-state allosteric model, to include geminate ligand rebinding and a structural relaxation following the photodissociation before any quaternary structural change.[41]

A particularly promising approach for the characterization of protein dynamics is based on the encapsulation in nanoporous silica gels. Solvent and small solute molecules can diffuse through the interconnected pores of the silica matrix, but the larger protein molecules are prevented from escaping into the surrounding buffer. It has been shown that not only do gel-encapsulated proteins retain their native structure and function but, in addition, their stability is usually enhanced.[42,43] Previous investigations demonstrated that Mb and Hb can be encapsulated in silica gels retaining spectroscopic and functional properties.[44−52] Gel encapsulation decreases the rates of quaternary structural rearrangements by several orders of magnitude, thus allowing the fixation of the protein into well-defined quaternary states on the time scale of kinetic and equilibrium experiments, as demonstrated for hemoglobin[46,48−55] and fructose-1,6-bisphosphatase.[56] These properties have allowed the characterization of rebinding kinetics to pure quaternary states of hemoglobin without the complication introduced by the overlapping quaternary transitions.[54,55] The gel structure can also effectively trap tertiary states of the proteins, as recently shown for myoglobin[57] and hemoglobin.[52,58]

The gel-encapsulated proteins constitute a promising experimental system for testing the effects of macromolecular crowding and molecular confinement on protein structure, function, and dynamics, as recently demonstrated for folding processes.[59,60] Gel encapsulation mimics the effects of confinement on the structure and stability of proteins and could thereby provide a suitable model system for the effects of crowding and confinement in a living cell. By using silica rather than a soluble macromolecule as the "crowding agent", it is possible to perturb the structure of the test protein without simultaneously affecting the structural integrity of the species that constitutes the crowded environment. Furthermore, intermolecular protein aggregation is prohibited in this system because the glass matrix shields the individual protein molecules from each other.

It is not clear yet how the gel matrix locks conformations characterized by different tertiary or quaternary structures. It is unlikely that these both static and dynamic effects are due to a simply higher viscosity of the medium, given the ease with which ligands enter and escape from the protein. For comparison, when COMb embedded in a highly viscous trehalose glass is photodissociated, the ligand cannot escape to the solvent even at room temperature, because the movements of the macromolecule are completely hindered.[61−63] The cavity surrounding the protein within the silica gels preferentially limits certain categories of conformational changes[43,57] and in some cases hinders molecular rotation.[64] Transitions between conformations that require a transition state with an enhanced volume and a change in the hydration pattern, as in hemoglobin,[25] may be especially vulnerable to being damped. This vulnerability could arise from both spatial constraints of the gel matrix and possible solvent shell effects by the negatively charged $Si-O^-$ groups lining the templated cavity surrounding the hydrated protein.[50,57] After wet-aging, gels shrink to 80−90% of their original volume, and the size of the protein-occupied pores is believed to be of the same order of magnitude as the diameter of the protein. It has been suggested that the protein itself may dictate the pore size during the gelation process.[47] A pore size distribution with an average value of 3−4 nm was reported for trypsin-doped xerogels using the BET and Kelvin equations from nitrogen adsorption isotherms.[65] A similar value (2−3 nm) was found for Hb-doped gels using transmission electron microscopy.[55]

In this work we have characterized the CO rebinding kinetics after photodissociation of horse heart Mb and human R-state Hb encapsulated in wet silica gels in the presence of various concentrations of glycerol. Glycerol has been extensively used as a cosolute in flash photolysis experiments on CO−heme-protein complexes in order to modulate the solution viscosity.[1−3,7−9,11,14,19,36,37,66,67]

A few investigations have already considered the effect of glycerol on the CO rebinding kinetics to gel-encapsulated hemoglobin[54] and myoglobin.[57] However, to our knowledge, this is the first attempt to describe quantitatively the effects on the rebinding kinetics. Our results provide evidence that besides viscosity, confinement and crowding effects are clearly discernible in the changes introduced by the gel matrix and glycerol on the CO rebinding kinetics to Mb and Hb.

Materials and Methods

Encapsulation of MbCO and R-State HbCO. A solution containing 10 mM HEPES and 1 mM EDTA (pH 6) was added to an equal volume of tetramethyl orthosilicate (TMOS) and vortexed for 2 min at 4 °C. The mixture was then deoxygenated by bubbling He for 90 min. An equal volume of a solution containing either 1% (w/v) hemoglobin or 1% (w/v) myoglobin, 10 mM HEPES, 1 mM EDTA, and 30 mM sodium dithionite (pH 6), saturated with CO, was added. The gelation occurred in 10−20 min at room temperature. When the gel was formed, a solution containing 100 mM HEPES, 1 mM EDTA, and 30 mM sodium dithionite (pH 7), saturated with CO, was layered on it. The sample thickness was ∼1 mm. Bathing solutions with concentrations of glycerol spanning from 10 to 80% (by weight) were employed. The gels thus obtained are transparent in the visible range, and their optical quality allows spectroscopic measurements. Samples were stored at 5 °C for 3 days before the kinetic experiments were performed to allow for equilibration of the system with CO in the gas phase. After this period, the kinetic traces were independent of aging (data not shown). Samples were kept at all stages in gastight vials to prevent O_2 leakage into the sample compartment. Absorbance spectra were routinely measured to ensure that the CO−protein complex was fully formed.[55,58]

Photolysis Setup. The sample was held in a 1 × 1 cm^2 gastight cuvette mounted in a homemade sample holder. The bathing solution was in equilibrium with a 1 atm CO atmosphere. Temperature was controlled by a peltier element with a feedback control mounted below the cuvette holder. This allowed temperature stability of better than 0.1 °C to be achieved in the temperature range of 10−50 °C. Dry gas flowing on the sample holder prevented condensation of humidity on the cuvette walls.

In the flash photolysis setup, photoexcitation was achieved using the second harmonic (532 nm) of a nanosecond Q-switched Nd:YAG laser (Quanta System Handy Yag HYL-101). Transient absorbance was monitored using a multiline, cw argon ion laser (Uniphase, 2013). The 488 nm line was selected by a Pellin Broca prism and an iris diaphragm. The power on the sample never exceeded 10 mW. Pump and probe beams hit the sample from the same side, approximately at right angles to the gel surface. The pump beam hit a relatively large sample area (7 mm diameter) containing the spot illuminated by the probe beam (1 mm diameter). Part of the excitation laser output was directed to an energy meter (Laser Precision RJ-7620) equipped with a pyroelectric energy probe (Laser Precision RJP-735). Experiments were conducted with laser pulse energies of ∼5 mJ. This energy corresponds to the photolysis of ≈30% of the CO-hemes, resulting in deoxy-heme concentrations of ∼100 μM at the end of the laser pulse. To minimize undesired photolysis of the samples due to the intense probe beam, a fast mechanical shutter (Uniblitz) was used. The HbCO samples were exposed for 600 ms, the MbCO samples were exposed for 300 ms, and the repetition rate of exposure cycles was ∼1 Hz. The synchronization of the experiment (laser triggering and shutter opening) was performed using home-built electronics.[68]

The probe beam was passed through a pinhole and a monochromator (Jobin Yvon H10 UV) for removing the stray light from the pump laser. The intensity of the transmitted light was measured by a Si avalanche photodiode (Hamamatsu S2382) coupled with a transimpedance amplifier (Avtech AV149). The voltage output was then recorded by a digital sampling oscilloscope (Lecroy LT374). Typically 100 traces were averaged to yield a transient absorbance signal. Three time scales were used, 1 μs div^{-1}, 100 μs div^{-1}, and 1 ms div^{-1}, and 10000 points were acquired for each trace.

Data Analysis. After preprocessing (baseline subtraction and pulse energy normalization), the transmitted intensity signal, $V(t)$, was converted to absorbance change, $\Delta A(t)$, with respect to the prepulse value (V_0) using the equation $\Delta A(t) = \log [V_0/V(t)]$. The absorbance change signals, corresponding to the different time scales, were merged into a single curve covering several time decades. Data were subsequently logarithmically down-sampled to give 200 point data sets. $\Delta A(t)$ values were then scaled to 1 to give the fraction of deoxy species, $N(t)$, as a function of time. The $\Delta A(t)$ signals at 488 nm contain no contributions from structural relaxation at the heme. This was verified by monitoring the rebinding kinetics of selected samples at the isosbestic wavelengths for the structural relaxations in myoglobin-doped (440 nm[11]) and R-state-hemoglobin-doped (436 nm[21,41]) gels. Signals were indistinguishable from those collected at 488 nm within the experimental errors (data not shown). Because the quality of the data at 488 nm was generally better, all of the experiments were performed at this wavelength.

The time course of $N(t)$ has been described by the sum of two stretched exponential functions

$$N(t) = A_g \exp\left[-\left(\frac{t - t_0}{\tau_g}\right)^{\beta_g}\right] + A_B \exp\left[-\left(\frac{t - t_0}{\tau_B}\right)^{\beta_B}\right] \quad (1)$$

where t_0 represents a horizontal offset, β_g and β_B are the stretching parameters, τ_g and A_g are the lifetime and the relative amplitude of the faster phase, respectively, and τ_B and A_B the lifetime and the amplitude of the slower phase. The sum of A_g and A_B is constrained to be equal to 1. Nonlinear least-squares fitting was performed using Origin 7.0. The goodness of the fits was judged from the value of reduced χ^2 and from visual inspection of the residuals.

We assume that the rate constant is the inverse of the average lifetime,[69] as given by

$$\langle \tau_i \rangle = \frac{\tau_i}{\beta_i \Gamma\left(\frac{1}{\beta_i}\right)} \quad (2)$$

where τ_i and β_i (i = g or B) are obtained from data fitting with the stretched exponential functions and $\Gamma(1/\beta_i)$ is the Γ function calculated at $1/\beta_i$. The temperature dependence of the rate constant is described by the Arrhenius equation

$$\ln(k) = \ln(k_0) - \frac{\Delta G^{\ddagger}}{RT} \quad (3)$$

where $\Delta G^{\ddagger}$ is the activation energy for the process, T is the temperature, and R is the gas constant.

To correct the observed activation energies for the contribution of the free energy of the ligand (vide infra), the solubility (s) of CO in glycerol−water mixtures was determined as a function of temperature, following a previously proposed protocol.[66] First, glycerol solutions were bubbled with pure gas under atmospheric conditions for 2−3 h with vigorous stirring. Then the vials were sealed and filled with 1 atm of CO, and the contents were left to equilibrate for 3 days at constant temperature. The procedure was repeated at different glycerol concentrations and temperatures. Aliquots of these solutions (60−200 μL) were withdrawn through a rubber septum and added to 3 mL of anaerobic solutions of deoxyhemoglobin. The concentration of CO in the original glycerol solution was calculated from the extent of HbCO formation. The resulting solubility values are shown in Figure 1.

The CO solubility at intermediate temperatures was estimated using an empirical relationship between s and the absolute temperature T, which models the temperature dependence of the solubility in each of the solvents in terms of an enthalpy difference (E_{CO}) between the CO in the gas phase and in the solvent:[11]

$$s(T) = s(273.16) \exp\left(\frac{E_{CO}}{R}\left(\frac{1}{T} - \frac{1}{273.16}\right)\right) \quad (4)$$

Results and Discussion

Rebinding of CO to heme-proteins encapsulated in wet silica gels after nanosecond laser photolysis occurs with two phases, corresponding to rebinding of CO from the protein matrix (geminate rebinding) and from the bulk solution (bimolecular rebinding), respectively.[54,55,57,70] The geminate rebinding, occurring on a sub-microsecond time scale, can be described as a first-order reaction with a time profile that can be correctly fit to a stretched exponential, to account for incomplete conformational substates averaging.[7,8,11,36] Under our experimental conditions (low photolysis level, large geminate rebinding) the

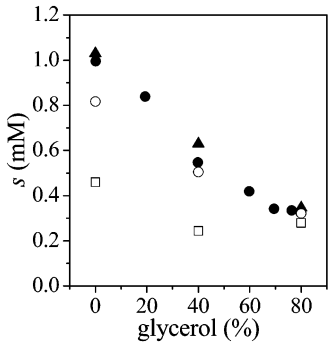

Figure 1. CO solubility in water−glycerol mixtures at different temperatures: $T = 10$ °C (▲), $T = 20$ °C (●, data from the literature[66]), $T = 25$ °C (○), $T = 65$ °C (□).

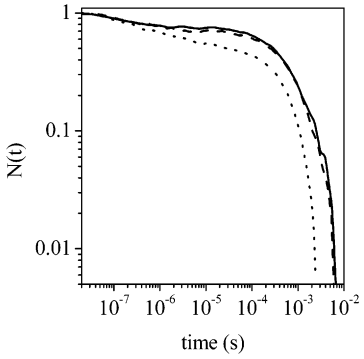

Figure 2. CO rebinding kinetics to horse heart MbCO encapsulated in wet silica gels, at 15 °C, in the absence (—) and presence of 40% (- - -) and 75% (···) glycerol concentrations.

bimolecular phase can be considered as a pseudo-first-order reaction, with the concentration of free CO being always at least a factor of 5 larger than the concentration of deoxy-hemes. We found that the bimolecular phase could be well described by a stretched exponential function. Equally good fits could be obtained with a sum of two exponential decay functions or the sum of two second-order functions. However, none of these fits proved to give meaningful results when analyzed in terms of microscopic rate constants. The need for the introduction of a stretching exponential could arise from some heterogeneity of the sample, resulting from either a static, or slowly relaxing, distribution of rates. If the latter were the case, these data would suggest that even on the time scale of bimolecular rebinding, conformational substate averaging is still incomplete.

The kinetics of CO rebinding to horse heart Mb gels at different glycerol concentrations and constant temperature, upon ligand photodissociation by a nanosecond laser pulse, are shown in Figure 2. The yield (Figure 5) and the lifetime (data not shown) of the geminate phase increase with glycerol concentration. On the other hand, the bimolecular phase shows a faster rebinding for samples bathed in a 75% glycerol buffer than for samples in aqueous solution.

CO rebinding kinetics to gel-encapsulated R-state Hb are shown in Figure 3 at selected glycerol concentrations. Although the changes in geminate rebinding resemble those observed for Mb (Figure 2), except for their absolute value, the bimolecular rebinding phase for Hb shows a qualitatively different behavior when glycerol is added. When the glycerol concentration in the buffer is increased, the geminate yield increases to 90% at 75% glycerol.

A temperature rise decreases the geminate yield and increases the bimolecular rebinding rate, as can be observed in Figure 4 for MbCO. The temperature dependence of CO rebinding

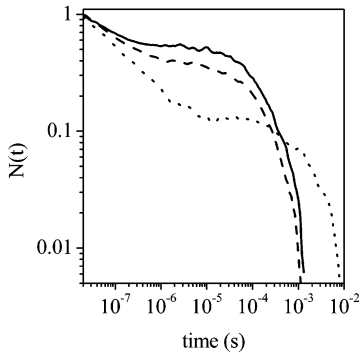

Figure 3. CO rebinding kinetics to R-state Hb encapsulated in wet silica gels, at 15 °C, in the absence (—) and presence of 40% (- - -) and 75% (···) glycerol concentrations.

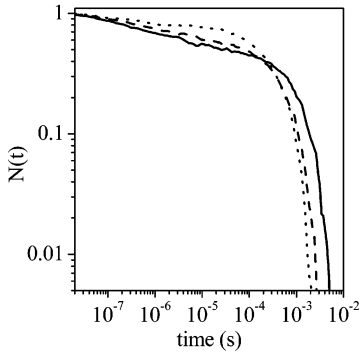

Figure 4. CO rebinding kinetics to horse heart Mb encapsulated in wet silica gels, at constant (80%) glycerol concentration. Kinetics are shown at three different temperatures: $T = 10$ °C (—), $T = 30$ °C (- - -), and $T = 50$ °C (···).

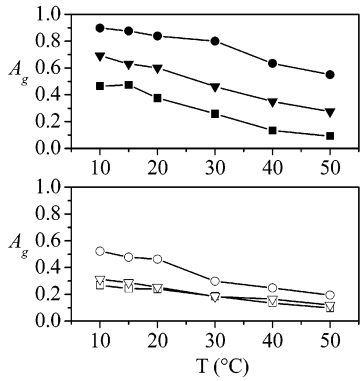

Figure 5. Geminate rebinding amplitudes for R-state HbCO (top, solid symbols) and MbCO (bottom, open symbols) gels as a function of the temperature at different glycerol concentrations in buffer: 0% (squares), 40% (triangles), and 75% (circles) glycerol.

kinetics to Hb-doped (data not shown) and Mb-doped gels is very similar. Figure 5 shows the variations with temperature of the amplitude A_g of the geminate phase for Mb and Hb gels, at selected glycerol concentrations. The presence of glycerol in the buffer increases the geminate yield for both myoglobin and hemoglobin, causing increases from 0.45 in aqueous buffer to 0.9 in 80% glycerol for HbCO and from 0.25 in aqueous buffer to 0.5 in 80% glycerol for MbCO gels at 15 °C. It is worthwhile comparing the geminate yield for gel-embedded MbCO and HbCO bathed in aqueous solutions at 15 °C, with the results obtained under the same conditions on gels prepared with a different encapsulation protocol. Our previous determination of the geminate yield for gel-embedded MbCO at 15 °C bathed in an aqueous solution gave a larger value for both sperm whale[55] and horse heart[70] MbCO. In those experiments we consistently

found values of 0.44 for both horse heart and sperm whale MbCO. The origin of the different yield of the geminate rebinding phase seems to reside in the encapsulation protocol we have used for the present experiments. At variance with previous preparations, in the present work the solutions containing tetramethyl orthosilicate were not sonicated. The geminate yield of our present MbCO samples is similar to the value reported by Friedman and co-workers[57] for samples prepared with a similar encapsulation protocol. Sonication of the TMOS solution is likely to lead to a more efficient formation of a sol, which can then proceed with higher yield to the formation of the gel network surrounding the protein. A more packed gel network around the protein is likely to be capable of wrapping the structure more efficiently and, hence, restraining the fluctuations that allow the CO to escape from the protein matrix to the solvent.

Interestingly, no similar effect was found for R-state HbCO samples for which the geminate yield is the same under the present and the former[55] experimental conditions, with a geminate yield of 0.45 at 15 °C for HbCO gels bathed in aqueous solutions. The larger size of the molecule, with a lower surface-to-volume ratio, the presence of intersubunit contacts, and the known specific interactions with water molecules are all possibly at the origin of the scarce sensitivity of the geminate yield to the encapsulation protocol. It has been reported that ≈15% of the hydrolyzed Si−O−Si linkages remain as Si−O$^-$ groups upon polycondensation, due to incomplete cross-linking during the gelation and aging steps of the sol−gel process.[71] The interaction with these residual charges on the gel matrix interface may also contribute to the observed different influence of the encapsulation on protein dynamics.

The apparent rates (τ_g and τ_B) and the geminate yields (A_g) for CO rebinding kinetics to gel-embedded HbCO and MbCO as a function of temperature and glycerol were determined from the fitting to eq 1. These values can be used to obtain rate constants for the elementary processes as outlined below. In the following, the apparent lifetimes (and rates) have been estimated from the fitting parameters using eq 2.[69]

Analysis of Microscopic Rates. In the simplest model,[4,36] the association reaction can be viewed as a pre-equilibrium between the intramolecular ligand position C and the dissociated state S in sequence with the bond formation of CO with heme iron, leading to the bound state A:

Scheme 2

$$\mathrm{A} \xleftarrow{k_{CA}} \mathrm{C} \underset{k_{SC}}{\overset{k_{CS}}{\rightleftharpoons}} \mathrm{S}$$

The elementary process $A \rightarrow C$, with rate constant k_{AC}, has been neglected. This model postulates two barriers to rebinding of CO at the heme iron: an inner barrier, which is a combination of electronic and steric factors, and an outer barrier for the passage of the ligand in and out of the protein. Scheme 2 is a simplified version of Scheme 1, where the states B, C, and D have been replaced by a single state C, identifying the CO inside the protein matrix without distinguishing between different docking positions. From state C, generated by nanosecond laser photolysis, the ligand either rebinds to the heme Fe (geminate rebinding) or escapes to the solvent. Depending on the relative height of the outer and inner barriers, the geminate yield can vary substantially. As explained in the Introduction, more complex kinetic schemes have been proposed, mainly for MbCO, where multiple substates are associated with the liganded protein (A) and the geminate couple (C).[1−3,7,9,11,14,36,39] However, in the limited temperature and viscosity ranges we have investigated with single-wavelength kinetics, we have no evidence that a more complex kinetic scheme is needed, and we assume that a three-state model constitutes a satisfactory minimal choice.

Although the CO rebinding kinetics in the case of Hb is more complex than for Mb, in some cases, it has been shown that, under specific experimental conditions, it can be treated with the simple three-state model.[17,18] Our choice of using a simplified kinetic scheme is justified by the fact that under our experimental conditions we have no quaternary changes following laser photolysis and the extended nature of the structural relaxation overlapping to the geminate rebinding can be described using a stretched exponential function.

The rate constants for the elementary processes in Scheme 2 are related to the measured rate constants (k_g and k_B) and the geminate yield (A_g). The rate constant of the geminate phase is given by a sum of the microscopic rate constants

$$k_g = k_{CA} + k_{CS} \tag{5}$$

and the amplitude of the geminate phase is given by

$$A_g = \frac{k_{CA}}{k_{CA} + k_{CS}} \tag{6}$$

where the contribution of CO molecules that come into the heme pocket from the solution can be neglected. The bimolecular step describes the CO rebinding from the solvent. A simple relationship between the bimolecular rate constant k_B (usually termed k_{ON}), the microscopic rate constant k_{SC}, and the geminate yield A_g can be obtained in the steady-state approximation:[4]

$$k_B = k_{SC} A_g \tag{7}$$

In this approximation, the concentration of protein in state C is assumed to be independent of time.[4] At [CO] = 1 mM, the relative values of the rate constants (*vide infra*) justify the steady-state approximation and show that during ligand rebinding there is a pre-equilibrium with respect to the CO entering and exiting a binding site in the protein.[4] The fraction of the occupied sites can be estimated to vary between 0.006 and 0.55% for HbCO gels and between 0.13 and 0.17% for MbCO gels. The lower limit is estimated at 10 °C and 80% glycerol, whereas the upper limit is calculated at 50 °C and 0% glycerol. The values of k_B are obtained as $1/[CO]\langle t_B \rangle$ using the solubility data in Figure 1.

We have investigated the response of the rebinding kinetics to changes in temperature and glycerol concentration. As discussed below, the effect of temperature and glycerol concentration is different on the various elementary processes.

The addition of glycerol to the bathing solution strongly affects the bulk viscosity of the solvent. According to the Kramers theory for the effect of solvent viscosity on unimolecular rate processes (k) in the condensed phase, an inverse proportionality is expected between the measured rate constants and solvent friction.[72] When protein conformational changes are expected to contribute to the observed kinetics, an additional source of friction, σ, has been envisioned, due to hindered intrachain motion within the protein. This friction adds to the friction from solvent molecules, η, at the protein surface in resisting protein relaxation after a perturbation as, for example, heme ligand photodissociation.[8] Under these conditions, the Kramers equation becomes

$$k(T,\eta) = \frac{C_a}{\sigma + \eta} e^{-E_a/RT} \quad (8)$$

where E_a is an activation energy and C_a is a proportionality factor.

Ansari et al.[8] showed that the data taken on MbCO in the temperature range between −5 and 35 °C could be well reproduced with $\sigma = 4.1 \pm 1.3$ cP. This value indicates that below ≈1 cP no effects are expected on the observed rates from changing solvent viscosity, whereas at viscosity above ≈15 cP the solvent friction dominates, thus reducing to the Kramers law.

In the case of gel-embedded HbCO and MbCO, it is possible to foresee an additional contribution to the internal friction σ, which may be associated with the effect of the gel matrix in slowing protein motions. The contribution from the gel is expected to be more effective on small proteins with large surface-to-volume ratios, where the interactions between the gel surrounding the protein and the protein surface are the largest. The geminate yield for HbCO is scarcely affected by the gel matrix,[54,55] indicating that the protein can fluctuate as if it was in a homogeneous solution, as far as the diffusion of the ligand in and out of the protein is concerned. On the contrary, the geminate yield for gel-embedded MbCO is much higher than it is in a homogeneous solution, suggesting that the gel matrix inhibits substantially the movements of the protein, which transiently open the exit channels and allow the ligand a very efficient escape route toward the solvent.[30] The internal friction due to the gel seems to be dependent on the molecular size.

Despite the obvious relevance of the internal microviscosity experienced by the macromolecules inside the gel pores in determining protein dynamical properties, only a few estimates have been given of this parameter.

Time-resolved fluorescence emission by gels doped with fluorescent probes allowed the determination of the local microviscosity inside gel pores.[73,74] Right after formation of the gel, the microviscosity, as sensed by the fluorescent probes Prodan and Rhodamine 6G, was characterized by a distribution centered at ≈2 cP. The microviscosity increased substantially with aging time, and the average of the distribution reached a value of $\approx 10^2$ cP. Upon the onset of water expulsion the width of the distribution decreased, illustrating a trend toward a more homogeneous microenvironment. Despite the increase in microviscosity with time, the initial value sensed by the fluorescent probes was invariably of a few centipoise, a value significantly lower than the average bulk viscosity.[75]

Figure 6 shows the rate coefficients k_{CA} as a function of solvent viscosity for MbCO and HbCO gels. The value we have used for the viscosity refers to the mixed solvent[76] bathing the gel and neglects contributions from the gel matrix, which are difficult, if not impossible, to determine. The values of k_{CA} for gel-embedded HbCO and MbCO (Figure 6) show a very weak dependence on η (and no dependence on temperature) in the relatively narrow viscosity (and temperature) range we have investigated, thus limiting the possibility to retrieve reliable parameters. However, for both systems it is clear that according to the model proposed by Ansari et al.[8] the internal friction for this process should be much higher than the friction of the bulk solvent in the investigated η range. In the case of HbCO gels we obtain $\sigma = 48 \pm 21$ cP, whereas for MbCO we have $\sigma = 15 \pm 6$ cP, averaged over the temperature range of 10−50 °C. There is no sign of significant temperature dependence of σ, as is also evident from the nearly perfect overlap between curves taken at different temperatures (Figure 6). In conclusion, the bulk viscosity has little influence on this process.

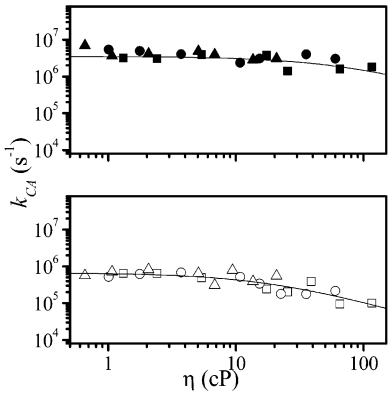

Figure 6. Rebinding rates k_{CA} versus solvent viscosity at 10 °C (squares), 20 °C (circles), and 40 °C (triangles) for HbCO (top, solid symbols) and MbCO (bottom, open symbols) gels. Gels are bathed in solutions at different glycerol concentrations (0−80% glycerol by weight). The range of the vertical scale is the same as that of Figure 7 to allow for an easier comparison. The solid lines are the result of the fit with eq 8 (see text).

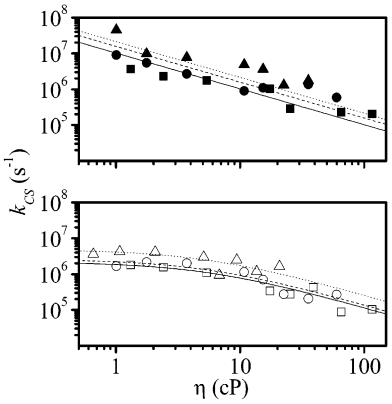

Figure 7. Ligand escape rates k_{cs} versus bulk solvent viscosity for HbCO (top, solid symbols) and MbCO (bottom, open symbols) gels at selected temperatures: $T = 10$ °C, squares; $T = 20$ °C, circles; $T = 40$ °C, triangles. The straight lines in the top plot are the fits using the Kramers model with η^{-1} slope: $T = 10$ °C, solid line; $T = 20$ °C, dashed line; $T = 40$ °C, dotted line; $R \geq 0.94$ in all cases. The fit for MbCO data ($T = 10$ °C, solid line; $T = 20$ °C, dashed line; $T = 40$ °C, dotted line) was performed using the modified expression (eq 8) for the viscosity dependence of the thermally activated rates for proteins, proposed by Ansari et al.[8] (see text).

The changes in the geminate yield (Figure 5) suggest that both glycerol concentration and temperature have effects on the rate coefficients characterizing the ligand escape to the solvent phase. In our simplified kinetic model, the origin of this dependence can be identified in the rate k_{CS}. The rate k_{CS} shows a large change as a function of the bulk solvent viscosity as shown in Figure 7 for HbCO and MbCO gels. This change is temperature dependent. As shown in Figure 7, the value of k_{CS} for HbCO gels decreases by 3 orders of magnitude when the glycerol concentration is increased from 0% (≈1 cP) to 80% (≈100 cP), whereas the corresponding decrease for MbCO gels occurs over only 2 orders of magnitude. At viscosities below ≈5 cP (i.e., at low glycerol concentrations) the change in k_{CS} is almost negligible.

The k_{CS} data for HbCO show a trend consistent with the η^{-1} slope predicted by the Kramers theory, and the corresponding linear fits are shown as the straight lines in the plot. This seems to point to a very small internal friction in the protein, with σ having a value below ≈1 cP at all temperatures. For gel-embedded HbCO the friction of the bulk solvent seems to be the dominant factor in slowing the k_{CS} rate at increasing glycerol

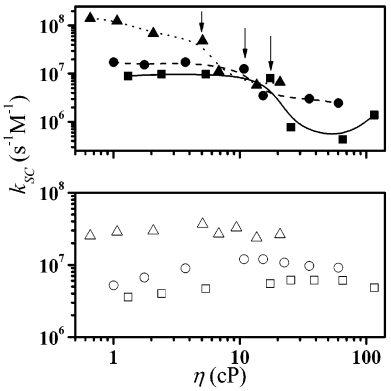

Figure 8. Ligand binding rates k_{SC} as a function of bulk solvent viscosity at selected temperatures for HbCO gels (top, solid symbols) and MbCO gels (bottom, open symbols): $T = 10$ °C, squares; $T = 20$ °C, circles; $T = 40$ °C, triangles. Solid lines in the top plot are intended only to guide the eye through the data points (40 °C, dotted line; 20 °C, dashed line; 10 °C, solid line). The arrows indicate the viscosity at which the abrupt change in k_{SC} for HbCO is observed.

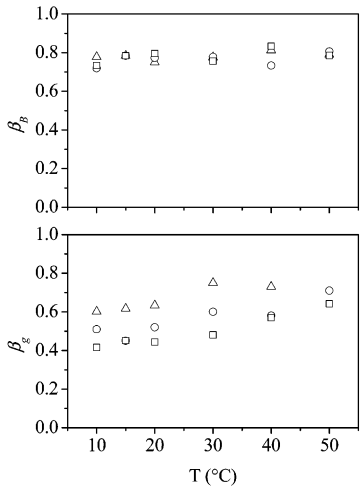

Figure 9. Temperature dependence of the stretching exponents β_g and β_B for gel-encapsulated MbCO at selected glycerol concentrations: 20%, △; 65%, ○; 80%, □.

concentrations. Although for HbCO the apparent agreement with the Kramers model holds across the whole viscosity range we have investigated, in the case of MbCO the η^{-1} slope is observed only above 10 cP and below 40 °C. In the case of MbCO gels, using eq 8 to fit the data in Figure 7, a value of $\sigma = 5.5 \pm 1.7$ cP has been estimated between 10 and 40 °C, in agreement with the value reported by Ansari et al. for MbCO in homogeneous solutions.[8] The proportionality factor C_a is temperature dependent (data not shown).

A complex and unexpected behavior was observed for k_{SC} when this rate was plotted as a function of the viscosity of the bathing solution. The rate k_{SC} for MbCO gels slightly increases at low viscosities, reaches a maximum corresponding to ≈70% glycerol, and then slowly decreases as the viscosity further increases. The curves are strongly temperature dependent, with rates generally increasing with temperature. In the case of HbCO gels, the rate constants decrease with increasing viscosity, then suddenly drop by almost a factor of 10 when the viscosity is increased above a "critical" value, corresponding to ≈60% glycerol. The value at which the rate shows the discontinuity is temperature dependent and is indicated by the arrows in Figure 8.

We will discuss these data in the following in terms of competitive effects of viscosity and enhanced activity of reactants due to molecular crowding and confinement.

It is worthwhile to point out that a similar trend of the rate constants k_{CA} and k_{CS} as a function of viscosity was observed previously for oxygen binding to hemerythrin following nanosecond laser flash photolysis.[77] In that case, the authors discussed the observed different viscosity dependence of the rate constants for the rebinding from the protein matrix and from the solution as arising from the different pathways followed by the ligand in the two processes. The authors concluded that hemerythrin undergoes a conformational transition upon ligand binding, which closes an exit channel necessary for ligand escape. A branched model has been recently proposed to explain the observed CO rebinding kinetics to Mb.[14,39] Further experiments in a wider viscosity range may help to assess if our data could support these models for MbCO.

Finally, it is worthwhile to compare the estimates of the microscopic rate constants for MbCO gels with the values determined by Henry et al.[4] The microscopic rates reported at $T = 22$ °C are as follows: $k_{CA} = (0.23 \pm 0.08) \times 10^6$ s^{-1}; $k_{CS} = (5.2 \pm 0.8) \times 10^6$ s^{-1}; and $k_{SC} = (5.2 \pm 0.8) \times 10^6$ M^{-1} s^{-1}. Our determinations show that in the gel the higher geminate rebinding arises from a higher $k_{CA} = (0.52 \pm 0.05) \times 10^6$ s^{-1} and a lower $k_{CS} = (1.7 \pm 0.2) \times 10^6$ s^{-1}, whereas rebinding from the bulk has essentially the same rate, $k_{SC} = (5.2 \pm 0.5) \times 10^6$ M^{-1} s^{-1}.

Temperature Dependence of β. The values of β_g and β_B obtained from the fits of the data are shown in Figure 9 for MbCO. Analogous results were obtained for HbCO gels. The value of β_B for both proteins is almost independent of temperature and glycerol concentration. On the contrary, the values of β_g increase toward 1 at increasing temperatures. Geminate yield decreases as the temperature is increased (Figure 5), and it is difficult to estimate β_g at high temperatures. When β_g values are compared at constant temperature as a function of glycerol concentration, we invariably find that the value of this parameter decreases as glycerol is added to the solution. This result can be compared to what is generally reported for the stretching exponent of the geminate rebinding to MbCO and HbCO in glycerol−water solutions at near-physiological temperatures. In the case of MbCO a stretching exponent of less than unity has been reported, but the data are scattered in a rather broad range (0.1−0.8)[9,11,35,36] The value of β_g for MbCO has been assumed to be independent of temperature and viscosity at physiological temperatures.[11] An explicit temperature dependence of the stretching parameter was observed previously in studies at low temperatures.[10,78] The temperature dependence of the stretching exponent for the geminate phase shows that protein relaxation and substate interconversion speed up to yield an almost exponential decay at high temperatures and suggests that a strong coupling may exist between the protein relaxation and the solvent shell or the gel matrix. The peculiar water structure in the pores[79] and the confinement of the protein inside a structure with a size comparable to the size of the protein may be at the origin of this behavior.[59,60]

Temperature Dependence of Rate Constants. The rate coefficient k_{CA} was found to be unaffected by temperature in the investigated range, within our experimental resolution. On the contrary, both k_{CS} and k_{SC} were found to be thermally activated. Figure 10 compares the Arrhenius plots for k_{CS} and k_{SC} for HbCO (top) and MbCO (bottom) at 40% glycerol. Within the limited temperature range we have investigated, the Arrhenius plots appear to be linear at all glycerol concentrations. It was previously reported that the temperature dependence of CO rebinding rate constants to myoglobin in viscous media can be

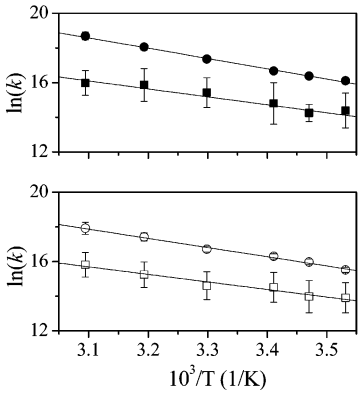

Figure 10. Arrhenius plot for k_{CS} (squares) and k_{SC} (circles) for HbCO (top, solid symbols) and MbCO (bottom, open symbols) at 40% glycerol. Error bars have been estimated form the errors associated with the parameters recovered from fitting.

appropriately described by Ferry's law.[7]

$$k = A\, e^{-(E_a/RT)^2} \tag{9}$$

However, in our limited temperature range, the nonlinearity in the Arrhenius plot implied by eq 9 is not evident. Attempts to fit the data using eq 9 did not yield meaningful results. Under our experimental conditions the rate constants can be adequately described with the Arrhenius model.

Because the temperature dependence of k_{CS} and k_{SC} follows an Arrhenius behavior under all investigated conditions, it was possible to give estimates of the activation barriers corresponding to the S → C and C → S microscopic processes as a function of the glycerol concentration in the bathing solution. These activation barriers for CO entrance into the protein and CO escape to solution are the free energy differences between the transition state and initial states, S and C, respectively. However, in the case of k_{SC}, data must be corrected for the changes in free energy of CO in solution as the glycerol concentration is increased, which leads to lower solubility values. The barriers for k_{SC} estimated from the Arrhenius plots contain a contribution from the chemical potential of the ligand, which should be removed in order to understand whether the addition of glycerol has any effect on the energetic barriers of the protein. As outlined under Materials and Methods, we have determined the solubility of CO in mixtures of glycerol and aqueous buffers at selected glycerol concentrations and temperatures. From these data, the values at intermediate glycerol concentrations and temperatures have been estimated. Following McKinnie and Olson,[66] we can write the free energy of the unliganded state as the sum of the energies of the reactants (protein and CO)

$$\Delta G^{\ddagger}_{SC} = G^{\ddagger}_{SC} - G_P - G_{CO} = \Delta G^{\ddagger}_{SC,P} - G_{CO} \tag{10}$$

where $\Delta G^{\ddagger}_{SC,P}$ represents the difference between the free energy of the transition state of the protein containing the ligand and that of the unliganded protein.

The solubility data allow a quantitative assessment of the change in the chemical potential of the free ligand with increasing glycerol concentration. If the value of G_{CO} for CO in buffer is defined as 0, then G_{CO} is given by

$$G_{CO} = RT \ln \frac{s_w}{s_g} \tag{11}$$

where s_w is the solubility in water and s_g the solubility in the glycerol solution.

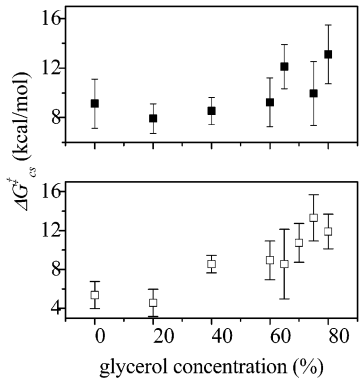

Figure 11. Activation energy barriers $\Delta G^{\ddagger}_{CS}$ relative to the CO escape into the solvent are shown as a function of glycerol concentration for HbCO (top) and MbCO gels (bottom).

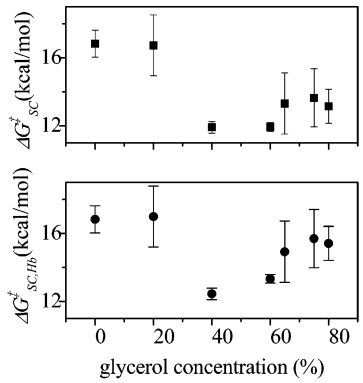

Figure 12. Activation energy barriers $\Delta G^{\ddagger}_{SC}$ (top) and $\Delta G^{\ddagger}_{SC,Hb}$ (bottom) are shown as a function of the glycerol concentration for HbCO gels.

The activation barriers $\Delta G^{\ddagger}_{CS}$ for the C → S step, obtained from the Arrhenius plots, are reported in Figure 11 as a function of glycerol concentration. The error bars on $\Delta G^{\ddagger}_{CS}$ (and on $\Delta G^{\ddagger}_{SC}$, vide infra) are estimated as the errors on the slopes of the Arrhenius plots. For both proteins $\Delta G^{\ddagger}_{CS}$ increases with the glycerol concentration, reflecting the increasing difficulty in finding escape routes to the solvent for the photodissociated CO. There are two main reasons for this increase in the barrier as glycerol is added to the bathing solution. First, the increased viscosity hinders the motions of the protein, allowing CO to exit to the solvent phase. Second, the decrease in CO solubility favors state C with respect to state S. The confinement of the proteins in the gel pores is possibly enhancing both effects.

The activation barriers $\Delta G^{\ddagger}_{SC,P}$ for the S → C step have been obtained as described above. It is interesting to compare the changes of $\Delta G^{\ddagger}_{SC}$ and $\Delta G^{\ddagger}_{SC,P}$ with glycerol concentration. The two parameters are shown in Figure 12 for HbCO gels as a function of glycerol concentration in solution. We find the presence of a minimum activation barrier corresponding to 40% glycerol in solution, for both $\Delta G^{\ddagger}_{SC}$ and $\Delta G^{\ddagger}_{SC,P}$. The correction for the changes in CO free energy does not remove this peculiar feature. Rather, it emphasizes this behavior by causing the barrier to increase at higher glycerol concentrations. The observed trend is at least surprising if we consider that the addition of glycerol should hinder the diffusion-mediated reactions, reduce reaction rates, and thus increase the energetic barriers for the process. The observed trend should therefore reflect some additional effects not described by the changes in viscosity of the bathing medium and in the solubility of CO.

The activation barriers $\Delta G^{\ddagger}_{SC}$ and $\Delta G^{\ddagger}_{SC,Mb}$ for gel-encapsulated MbCO samples are shown in Figure 13. Also for MbCO

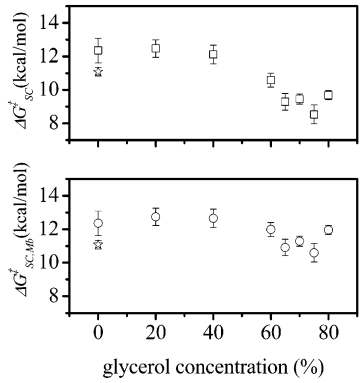

Figure 13. Activation energy barriers $\Delta G^{\ddagger}_{SC}$ (top) and $\Delta G^{\ddagger}_{SC,Mb}$ (bottom) are shown as a function of the glycerol concentration for MbCO gels. The stars are the corresponding activation energies for MbCO in aqueous solution.

gels we observe the presence of a minimum barrier for $\Delta G^{\ddagger}_{SC}$ corresponding to 75% glycerol concentration, although the minimum is less pronounced than for HbCO gels. Our estimates for the barriers $\Delta G^{\ddagger}_{SC}$ and $\Delta G^{\ddagger}_{CS}$ in 75% glycerol are in very good agreement with previous determinations for aqueous solutions of human MbCO in the presence of the same concentration of glycerol. For these samples, values of $\Delta G^{\ddagger}_{CS} = 14.6$ and $\Delta G^{\ddagger}_{SC} = 9.5$ kcal/mol were estimated.[36] A similarly good agreement is observed between the activation barriers $\Delta G^{\ddagger}_{SC}$ and $\Delta G^{\ddagger}_{SC,Mb}$ for MbCO in aqueous solution (shown as the stars in Figure 13) and the corresponding barriers for the gel-encapsulated sample.

The behavior observed for the rate constant of the elementary processes S → C and C → S of Hb and Mb gels bathed in viscous media can be rationalized by considering the opposing effects of increasing the concentration of cosolutes (glycerol) which, at the same time, affects the activity of the reactants, the solubility of CO, and the viscosity of the medium. When cosolutes are present at high concentrations, the volume available to diffusion of reactants participating in a chemical reaction is dramatically decreased, due to the mutual impenetrability of all solute molecules. This effect is often referred to as molecular crowding.[80−84] This nonspecific steric repulsion is always present, regardless of any other attractive or repulsive interactions that might occur between solute molecules. Moreover, the gel matrix, in which the proteins are dispersed in small elements or pores, with dimensions comparable to the size of the protein, acts as a crowded medium in which the crowding agent is the gel matrix itself.[59,60] The available volume per macromolecule thus defines an effective concentration that can be much higher than the actual one, and the activity coefficient thus increases dramatically in the crowded medium. The effects of crowding on biochemical reaction rates are complex, because although crowding reduces diffusion, it increases thermodynamic activities. The net result of these opposing effects depends on the precise nature of each reaction. According to the transition-state theory, reactions can be either transition-state limited or diffusion limited. For a diffusion-limited reaction, which is limited by the reactants' encounter rate, crowding will reduce the overall rate by reducing diffusion. For a transition-state-limited reaction, which is limited by the activity of the encounter complex, crowding will increase the rate constant because crowding increases the activity. The maximum possible rate for any multimolecular reaction is ultimately set by the encounter rate of the components, so even for a transition-state-limited reaction, the rate will eventually fall as crowding increases.

The CO rebinding to Hb and Mb is a transition-state-limited reaction,[30] and the rebinding rate constants are expected to show a biphasic behavior as the crowding agent (glycerol) is added (Figure 8).[80]

When the rate constant k_{SC} for HbCO and MbCO gels is plotted as a function of the concentration of the crowding agent, the observed biphasic behavior is compatible with what would be expected for reaction kinetics occurring in a crowded medium.

The minimum in activation energy in Figure 12 for the S → C process can be rationalized as due to the superposition of the two effects of molecular crowding: an increase of the reactants activity, which energetically makes the reaction easier, and a viscous dissipation that hinders reactants motions and thus increases the reaction barrier. When the glycerol concentration is high enough, the effect of viscosity prevails, increasing the corresponding activation barrier.

The effects of molecular crowding for the microscopic process C → S in both proteins act in the same direction. This means that the presence of a crowding agent both increases the activity of the reactants and makes the reactants' movements difficult, and, consequently, stabilizes state C under all conditions.

Conclusions

We have investigated the CO rebinding kinetics to gel-embedded Mb and Hb after nanosecond flash photolysis in the presence of glycerol (from 0 to 80 wt %), in the temperature range of 10−50 °C. The geminate yield for HbCO is scarcely affected by the gel matrix. On the contrary, the geminate yield for gel-embedded MbCO is much higher than that in solution, suggesting that the gel matrix inhibits substantially the movements of the protein. A strong enhancement of the geminate yield is observed for both proteins when glycerol concentration is increased and temperature is decreased. The observed rebinding kinetics have been rationalized with a simple three-state kinetic model. Rate constants have been modeled using a modified Kramers equation, indicating that the gel exerts an internal friction on the elementary rate constants. The extent of this friction is different for the various microscopic processes and likely reflects contributions from the peculiar water structure in the gel pores. The effects of glycerol on the rate constant k_{CA} are scarce and indicate a high internal friction, essentially temperature independent, for both proteins. The internal friction for the ligand escape rate, k_{CS}, is much smaller and is found to be negligible for HbCO and ∼5 cP for MbCO. The activation barrier for k_{CS} increases with glycerol concentration due to increased viscosity and reduced ligand solubility. The rate k_{SC} shows a complex behavior that reflects the opposing effects of viscosity and activity due to molecular confinement and crowding. Accordingly, the corresponding activation barriers show a biphasic behavior, with a minimum at ≈40% glycerol for HbCO and at ≈75% glycerol for MbCO.

Acknowledgment. We thank MIUR (C.V., COFIN 2001) and INFM (C.V. and A.M., FIRB nanotechnologies) for financial support.

References and Notes

(1) Austin, R. H.; Beeson, K. W.; Eisenstein, L.; Frauenfelder, H.; Gunsalus, I. C. *Biochemistry* **1975**, *14*, 5355−5373.

(2) Beece, D.; Eisenstein, L.; Frauenfelder, H.; Good, D.; Marden, M. C.; Reinisch, L.; Reynolds, A. H.; Sorensen, L. B.; Yue, K. T. *Biochemistry* **1980**, *19*, 5147−5157.

(3) Doster, W.; Beece, D.; Bowne, S. F.; DiIorio, E. E.; Eisenstein, L.; Frauenfelder, H.; Reinisch, L.; Shyamsunder, E.; Winterhalter, K. H.; Yue, K. T. *Biochemistry* **1982**, *21*, 4831−4839.

(4) Henry, E. R.; Sommer, J. H.; Hofrichter, J.; Eaton, W. A. *J. Mol. Biol.* **1983**, *166*, 443−451.

(5) Ansari, A.; Berendzen, J.; Bowne, S. F.; Frauenfelder, H.; Iben, I. E. T.; Sauke, T. B.; Shyamsunder, E.; Young, R. D. *Biochemistry* **1985**, *24*, 5000−5004.

(6) Srajer, V.; Reinisch, L.; Champion, P. M. *J. Am. Chem. Soc.* **1988**, *110*, 6656−6670.

(7) Steinbach, P. J. *Biochemistry* **1991**, *30*, 3988−4001.

(8) Ansari, A.; Jones, C. M.; Henry, E. R.; Hofrichter, J.; Eaton, W. *Science* **1992**, *256*, 1796−1798.

(9) Tian, W. D.; Sage, J. T.; Srajer, V.; Champion, P. M. *Phys. Rev. Lett.* **1992**, *68*, 408−411.

(10) Post, F.; Doster, W.; Karvounis, G.; Settles, M. *Biophys. J.* **1993**, *64*, 1833−1842.

(11) Ansari, A.; Jones, C. M.; Henry, E. R.; Hofrichter, J.; Eaton, W. *Biochemistry* **1994**, *33*, 5128−5145.

(12) Chen, E.; Goldberg, R. A.; Kliger, D. S. *Annu. Rev. Biophys. Biomol. Struct.* **1997**, *26*, 327−355.

(13) Esquerra, R. M.; Goldbeck, R. A.; Kim-Shapiro, D. B.; Kliger, D. S. *Biochemistry* **1998**, *37*, 17527−17536.

(14) Kleinert, T.; Doster, W.; Leyser, H.; Petry, W.; Schwarz, V.; Settles, M. *Biochemistry* **1998**, *37*, 717−733.

(15) McMahon, B. H.; Stojkovic, B. P.; Hay, P. J.; Martin, R. L.; Garcia, A. E. *J. Chem. Phys.* **2000**, *113*, 6831−6850.

(16) Hofrichter, J.; Sommer, J. H.; Henry, E. R.; Eaton, W. A. *Proc. Natl. Acad. Sci. U.S.A.* **1983**, *80*, 2235−2239.

(17) Murray, L. P.; Hofrichter, J.; Henry, E. R.; Eaton, W. A. *Biophys. Chem.* **1988**, *29*, 63−76.

(18) Murray, L. P.; Hofrichter, J.; Henry, E. R.; Ikeda-Saito, M.; Kitagishi, K.; Yonetani, T.; Eaton, W. A. *Proc. Natl. Acad. Sci. U.S.A.* **1988**, *85*, 2151−2155.

(19) Findsen, E. W.; Friedman, J. M.; Ondrias, M. R. *Biochemistry* **1988**, *27*, 8719−8724.

(20) Jones, C. M.; Ansari, A.; Henry, E. R.; Christoph, G. W.; Hofrichter, J.; Eaton, W. A. *Biochemistry* **1992**, *31*, 6692−6702.

(21) Henry, E. R.; Jones, C. M.; Hofrichter, J.; Eaton, W. A. *Biochemistry* **1997**, *36*, 6511−6528.

(22) Bjorling, S. C.; Goldbeck, R. A.; Paquette, S. J.; Milder, S. J.; Kliger, D. S. *Biochemistry* **1996**, *35*, 8619−8627.

(23) Goldbeck, R. A.; Paquette, S. J.; Björling, S. C.; Kliger, D. S. *Biochemistry* **1996**, *35*, 8628−8639.

(24) Esquerra, R. M.; Goldbeck, R. A.; Reaney, S. H.; Batchelder, A. M.; Wen, Y.; Lewis, J. W.; Kliger, D. S. *Biophys. J.* **2000**, *78*, 3227−3239.

(25) Goldbeck, R. A.; Paquette, S. J.; Kliger, D. S. *Biophys. J.* **2001**, *81*, 2919−2934.

(26) Schlichting, I.; Berendzen, J.; Phillips, G. N.; Sweet, R. M. *Nature* **1994**, *371*, 808−812.

(27) Hartmann, H.; Zinser, S.; Komninos, P.; Schneider, R. T.; Nienhaus, G. U.; Parak, F. *Proc. Natl. Acad. Sci. U.S.A.* **1996**, *93*, 7013−7016.

(28) Chu, K.; Vojtchovsky, J.; McMahon, B. H.; Sweet, R. M.; Berendzen, J.; Schlichting, I. *Nature* **2000**, *403*, 921−923.

(29) Ostermann, A.; Washipky, R.; Parak, F. G.; Nienhaus, G. U. *Nature* **2000**, *404*, 205−208.

(30) Olson, J. S.; Phillips, G. N. J. *J. Biol. Chem.* **1996**, *271*, 17593−17596.

(31) Eaton, W. A.; Henry, E. R.; Hofrichter, J.; Mozzarelli, A. *Nat. Struct. Biol.* **1999**, *6*, 351−358.

(32) Lim, M.; Jackson, T. A.; Anfinrud, P. A. *Proc. Natl. Acad. Sci. U.S.A.* **1993**, *90*, 5801−5804.

(33) Jackson, T. A.; Lim, M.; Anfinrud, P. A. *Chem. Phys.* **1994**, *180*, 131−140.

(34) Agmon, N.; Hopfield, J. *J. Chem. Phys.* **1983**, *79*, 2042−2053.

(35) Hagen, S. J.; Eaton, W. A. *J. Chem. Phys.* **1996**, *104*, 3395−3398.

(36) Balasubramanian, S.; Lambright, D. G.; Marden, M. C.; Boxer, S. G. *Biochemistry* **1993**, *32*, 2202−2212.

(37) Frauenfelder, H.; Alberding, N. A.; Ansari, A.; Braunstein, D.; Cowen, B. R.; Hong, M. K.; Iben, I. E. T.; Johnson, J. B.; Luck, S.; Marden, M. C.; Mourant, J. R.; Ormos, P.; Reinisch, L.; Scholl, R.; Schulte, A.; Shyamsunder, E.; Soremen, L. B.; Steinbach, P. J.; Xie, A.; Young, R. D.; Yue, K. T. *J. Phys. Chem.* **1990**, *94*, 1024−1037.

(38) Frauenfelder, H.; Sligar, S. G.; Wolynes, P. G. *Science* **1991**, *254*, 1598−1603.

(39) Angeloni, L.; Feis, A. *Photochem. Photobiol. Sci.* **2003**, *2*, 730−740.

(40) Lyons, K. B.; Friedman, J. M. In *Hemoglobin and Oxygen Ginding*; Ho, C., Eaton, W. A., Collman, J. P., Gibson, Q. H., Leigh, J. S., Margolias, E., Moffat, K., Scheidt, W. R., Eds.; Elsevier/North-Holland: Amsterdam, The Netherlands, 1982.

(41) Henry, E. R.; Bettati, S.; Hofrichter, J.; Eaton, W. A. *Biophys. Chem.* **2002**, *98*, 149−164.

(42) Mozzarelli, A.; Bettati, S. In *Advanced Functional Molecules and Polymers*; Nalwa, H. S., Ed.; Overseas Publishers Association: Tokyo, 2001; Vol. 4, pp 55−97.

(43) Bettati, S.; Pioselli, B.; Campanini, B.; Viappiani, C.; Mozzarelli, A. In *Encyclopedia of Nanoscience and Nanotechnology*; Nalwa, H. S., Ed.; American Scientific Publishers: Stevenson Ranch, CA, 2004; Vol. 10, pp 1−23.

(44) Ellerby, L.; Nishida, C. R.; Nishida, F.; Yamanaka, S. A.; Dunn, B.; Valentine, J. S.; Zink, J. I. *Science* **1992**, *255*, 1113−1115.

(45) Dave, B. C.; Dunn, B.; Valentine, J. S.; Zink, J. I. *Anal. Chem.* **1994**, *66*, 1120A.

(46) Shibayama, N.; Saigo, S. *J. Mol. Biol.* **1995**, *251*, 203−209.

(47) Lan, E. H.; Dave, B. C.; Fukuto, J. M.; Dunn, B.; Zink, J. I.; Valentine, J. S. *J. Mater. Chem.* **1999**, *9*, 45.

(48) Shibayama, N.; Saigo, S. *J. Am. Chem. Soc.* **1999**, *121*, 444−445.

(49) Bettati, S.; Mozzarelli, A. *J. Biol. Chem.* **1997**, *272*, 32050−32055.

(50) Das, T. K.; Khan, I.; Rousseau, D.; Friedman, J. M. *Biospectroscopy* **1999**, *5*, S64−S70.

(51) Juszczak, L. J.; Friedman, J. M. *J. Biol. Chem.* **1999**, *274*, 30357−30360.

(52) Shibayama, N.; Saigo, S. *FEBS Lett.* **2001**, *429*, 50−53.

(53) Shibayama, N.; Saigo, S. *J. Am. Chem. Soc.* **1999**, *121*, 444−445.

(54) Khan, I.; Shannon, C. F.; Dantsker, D.; Friedman, A. J.; Perez-Gonzales-de-Apodaca, J.; Friedman, J. M. *Biochemistry* **2000**, *39*, 16099−16109.

(55) Abbruzzetti, S.; Viappiani, C.; Bruno, S.; Bettati, S.; Bonaccio, M.; Mozzarelli, A. *J. Nanosci. Nanotechnol.* **2001**, *1*, 407−415.

(56) McInninch, J. K.; Kantrowitz, E. R. *Biochim. Biophys. Acta−Protein Struct. Mol. Enzymol.* **2001**, *1547*, 320−328.

(57) Samuni, U.; Dantsker, D.; Khan, I.; Friedman, A. J.; Peterson, E.; Friedman, J. M. *J. Biol. Chem.* **2002**, *277*, 25783−25790.

(58) Bruno, S.; Bonaccio, M.; Bettati, S.; Rivetti, C.; Viappiani, C.; Abbruzzetti, S.; Mozzarelli, A. *Protein Sci.* **2001**, *10*, 2401−2407.

(59) Eggers, D. K.; Valentine, J. S. *Protein Sci.* **2001**, *10*, 250−261.

(60) Eggers, D. K.; Valentine, J. S. *J. Mol. Biol.* **2001**, *314*, 911−922.

(61) Hagen, S. J.; Hofrichter, J.; Eaton, W. A. *J. Phys. Chem.* **1996**, *100*, 12008−12021.

(62) Hagen, S. J.; Hofrichter, J.; Eaton, W. A. *Science* **1995**, *269*, 959−962.

(63) Librizzi, F.; Viappiani, C.; Abbruzzetti, S.; Cordone, L. *J. Chem. Phys.* **2002**, *116*, 1193−1200.

(64) Gottfried, D. S.; Kagan, A.; Hoffman, B. M.; Friedman, J. M. *J. Phys. Chem. B* **1999**, *103*, 2803−2807.

(65) Shtelzer, S.; Rappoport, S.; Avnir, D.; Ottolenghi, M.; Braun, S. *Biotechnol. Appl. Biochem.* **1992**, *15*, 227−235.

(66) McKinnie, R. E.; Olson, J. S. *J. Biol. Chem.* **1981**, *256*, 8928−8932.

(67) Tian, W. D.; Sage, J. T.; Champion, P. M.; Chien, E.; Sligar, S. G. *Biochemistry* **1996**, *35*, 3487−3502.

(68) Banderini, A.; Sottini, S.; Viappiani, C. *Rev. Sci. Instrum.* **2004**, in press.

(69) Lindsey, C. P.; Patterson, G. P. *J. Chem. Phys.* **1980**, *73*, 3348−3357.

(70) Abbruzzetti, S.; Viappiani, C.; Bruno, S.; Mozzarelli, A. *Chem. Phys. Lett.* **2001**, *346*, 430−436.

(71) Reetz, M. T.; Zonta, A.; Simpelkamp, J.; Rufinska, A.; Tesche, B. *J. Sol-Gel Sci. Technol.* **1996**, *7*, 35−43.

(72) Kramers, H. A. *Physica* **1940**, *7*, 284−304.

(73) Narang, U.; Jordan, J. D.; Bright, F. V.; Prasad, P. N. *J. Phys. Chem.* **1994**, *98*, 8101−8107.

(74) Narang, U.; Wang, R.; Prasad, P. N.; Bright, F. V. *J. Phys. Chem.* **1994**, *98*, 17.

(75) Kozuka, H.; Kurori, H.; Sakka, S. *J. Non-Crystalline Solids* **1987**, *95/96*, 1181−1188.

(76) Miner, C. S., Dalton, N. N., Eds. *Glycerol*; Reinhold: New York, 1953.

(77) Lavalette, D.; Tetreau, C. *Eur. J. Biochem.* **1988**, *177*, 97−108.

(78) Agmon, N.; Doster, W.; Post, F. *Biophys. J.* **1994**, *66*, 1612−1622.

(79) Navati, M. S.; Ray, A.; Shamir, J.; Friedman, J. M. *J. Phys. Chem. B* **2004**, *108*, 1321−1327.

(80) Ellis, R. J. *Trends Biochem. Sci.* **2001**, *26*, 597−604.

(81) Minton, A. P. *Biopolymers* **1981**, *20*, 2093−2120.

(82) Minton, A. P. *Int. J. Biochem.* **1990**, *22*, 1063−1067.

(83) Minton, A. P. *J. Biol. Chem.* **2001**, *276*, 10577−10580.

(84) Ellis, R. J. *Curr. Opin. Struct. Biol.* **2001**, *11*, 114−119.